American Society of Mechanical Engineers

ASME Accepted Manuscript Repository

Institutional Repository Cover Sheet

First Last

ASME Paper Title: Total focusing method based ultrasonic phased array imaging in thick structures

Authors: Sumana and Anish Kumar

ASME Journal Title: Journal of Nondestructive Evaluation, Diagnostics and Prognostics of Engineering Systems

Volume/Issue 4(4) Date of Publication (VOR* Online) 04/05/2021

ASME Digital Collection URL: https://asmedigitalcollection.asme.org/nondestructive/article-abstract/4/4/041005/1106549/Total-Focusing-Method-Based-Ultrasonic-Phased?redirectedFrom=fulltext

DOI: **10.1115/1.4050802**

ASME ©; CC-BY 4

*VOR (version of record)

Sumana, S., & Kumar, A. (2021). Total focusing method-based ultrasonic phased array imaging in thick structures. *Journal of Nondestructive Evaluation, Diagnostics and Prognostics of Engineering Systems*, *4*(4), [041005]. https://doi.org/10.1115/1.4050802

TOTAL FOCUSING METHOD BASED ULTRASONIC PHASED ARRAY IMAGING IN THICK STRUCTURES

Sumana[#] and Anish Kumar*
Nondestructive Evaluation Division
Metallurgy and Materials Group
Indira Gandhi Centre for Atomic Research
Homi Bhabha National Institute
Kalpakkam-603 102, Tamil Nadu, India
* *anish@igcar.gov.in*
[#] sumana.sumana@strath.ac.uk

Abstract

Ultrasonic non-destructive testing traditionally uses a conventional monolithic transducer. An approach similar to this comprising of independent single transmissions but with reception performed by all the elements in phased array ultrasonics is known as Full Matrix Capture (FMC). The acquired data is processed by Total Focusing Method (TFM). Conventional FMC-TFM has limitations in the inspection at large depth in attenuating materials due to single element transmission. To improve the beam forming process, coherent recombination of the plane wave with specific angles is utilized in transmission and the same aperture is used for the reception in Plane Wave Imaging (PWI). A new methodology called Angle Beam Virtual Source FMC-TFM (ABVSFMC-TFM) is proposed to inspect thick attenuating materials such as nickel base alloys. The ABVSFMC method leads to improved Signal to Noise Ratio (SNR) as compared to the conventional FMC due to increased energy with directivity during transmission using a group of elements and improved divergence as compared to the PWI due to a small virtual source near the sample surface.

In the present paper, FMC-TFM, PWI-TFM and ABVSFMC-TFM methods are compared for inspection of thick nickel base superalloy (Alloy 617) with slots at various depths in the range of 25-200 mm. Optimization of the incidence angle has been performed by beam computation in CIVA software. Results obtained by CIVA simulations are discussed and also compared for the three methods.

Keywords: FMC-TFM, VSFMC-TFM, PWI, phased array

1. INTRODUCTION

Phased array ultrasonic technique (PAUT) based inspections are replacing the other volumetric inspection methods in nondestructive testing including conventional ultrasonics and radiography. Full Matrix Capture–Total Focusing Method (FMC-TFM) is one of the most advanced methods in PAUT and is called a 'gold standard' method [1]. FMC is performed by acquiring data from each possible pulse-receive combination of the transducer array. All elements are utilized as transmitters sequentially to obtain N*N numbers of A-scan signals for a transducer with N elements [2]. The raw A-scan signals are processed by Total Focusing Method (TFM). FMC-TFM has limitations in the inspection at large depth in thick attenuating materials as a single element transmission limits the penetration of sound beam especially at larger depths [3]. FMC-TFM inspection also poses problem for the inspection of weld joints. Linear array cannot be placed on top of the weld bead. Angle beam FMC-TFM reduces the sensitivity further due to additional interfaces and wedge material. Karaman et al. [4] proposed the concept of 'virtual source'. The data acquisition is performed using a group of elements that form a virtual focusing above [5, 6] or below [7] the surface of the specimen. Acoustic energy produced by the virtual source is higher and enables the

inspection at large depth with improved Signal to Noise Ratio (SNR). TFM performance speed can be enhanced by reducing the number of independent firings [8, 9]. However, without optimization of the transducer parameters, sparse array may produce the side lobe or grating lobes [1]. Bannouf et al. [8] compared the FMC-TFM, Sparse Matrix Capture (SMC) and Virtual Sparse Array (VSA) for Side Drill Holes (SDHs) of 2 mm diameter up to 75 mm depth in a ferritic steel specimen. Signal loss was observed in FMC-TFM method due to material presenting high level of structural noise and to overcome the problem, VSA method was utilized. Spencer et al. [2] compared the advanced ultrasonic techniques such as Phased Array (PA), FMC-TFM and Advanced Focusing Method (AFMC-TFM) for the inspection of Electrical Discharge Machined (EDM) notches in weld region of flat carbon steel plates of 19 mm thickness. It was observed that the smooth fracture face of vertical notches could not be detected by any of the above techniques. Long et al. [3] utilized reflected and mode converted waves for the inspection of two flat bottom holes representing a lack of fusion in the weld region using FMC-TFM technique. Experimental results showed that with 32 elements aperture size, only the top tip signals could be observed.

The transmission energy can be increased by employing Plane Wave Imaging (PWI), where all the elements are fired simultaneously to generate a plane wave. Simultaneous transmission of the elements with high acoustic power results in improved sensitivity. As the divergence of the plane wave is very limited, suitable delay laws are applied to sweep the plane waves at different angles and data is received by all the elements [13-16]. Recently, direct and half skip mode PWI have been utilised for the inspection of irregular surfaces. Simulation was performed using CIVA software for the validation for point like and crack like defects [14]. Long et al. [4] have also performed CIVA simulation of FMC-TFM imaging for structurally complex stainless-steel piping

of 50 mm thickness. A good agreement was observed between the simulation and the experimental results in presence of weld anisotropy.

The success of a TFM based technique (FMC or PWI) depends upon the number of A-scans in which the flaw information is present. Larger the number of A-scans with flaw information, better is the focusing or beam forming achieved. In case of FMC-TFM, this is achieved with the help of the large divergence of the beam emanating from a transducer element of small width and multiple receivers. In PWI, this is achieved by multiple receivers and transmitting plane waves at smaller angular steps. With increasing depth of inspection, smaller angular steps may be required. Further, PWI technique requires a phased array equipment with a larger number of simultaneous pulser channels. An alternate technique, Angle Beam Virtual Source (ABVS) FMC-TFM having a few advantages of both the FMC and the PWI techniques is explored in the present study and the results are compared with those obtained by FMC-TFM and PWI techniques. The ABVSFMC-TFM is proposed to enhance the sensitivity and SNR during ultrasonic inspection of thick narrow gap weld joints of austenitic nickel base super alloys. Ultrasonic inspection of thick austenitic steel and nickel base superalloys poses specific challenges due to large elastic anisotropy and coarse grains in the weld metal [5]. Hence, thick austenitic welds cannot be inspected using normal beam inspection. As a group of elements is used in transmission in the ABVSFMC-TFM, a divergent beam of increased amplitude as compared to FMC with specific directivity can be achieved without using a wedge. Optimization of the incidence angle is performed in the present study by beam computation in CIVA software. The methodology is simulated in CIVA software for different angles by imaging the tip diffracted signals obtained from slot type planar defects at various depths in the range of 25-175 mm in a 200 mm thick nickel base superalloy (Alloy 617) forging. Also, the simulation and experimental results are compared with those of PWI and FMC-TFM.

2. MATERIALS AND METHODS

2.1 Specimen details:

An Alloy 617 calibration block of dimensions 200 mm (h) * 75 mm (w) * 370 mm (l) as shown in Fig. 1 is used for CIVA simulation and experimental studies. The specimen comprises of six numbers of 25 mm deep Side Drill Holes (SDHs) and seven numbers of 25 mm deep slots at different heights on the two opposite faces of the block, as shown in Fig. 1. The top three SDHs (at 25 mm, 50 mm and 75 mm from the top surface) are of 4 mm diameter, whereas, the bottom three SDHs are of 6 mm diameter. Similarly, the top three slots are of 4 mm height and the bottom three vertical slots are of 6 mm height. The width of the horizontal slot at 150 mm depth is 6 mm. The vertical slots simulate lack of sidewall fusion in a narrow gap thick weld joint and the horizontal slot simulates an inter-pass slag/oxide layer. Due to the difficulty in machining deep slots in a nickel base superalloy, the minimum possible width of the notch could only be achieved as 1 mm practically by electrode discharge machining (EDM).

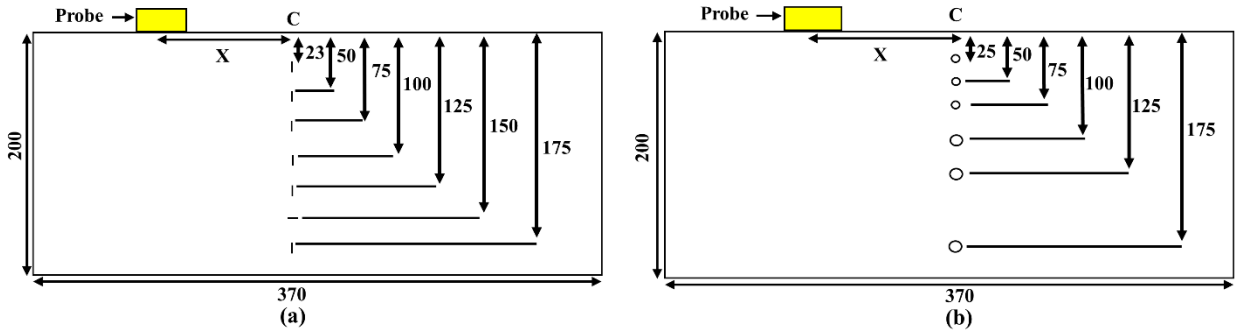

Figure 1. Schematic of Alloy 617 specimen showing (a) planar defects and (b) side drill holes on the two opposite faces.

2.2 CIVA simulation and experimental details:

A 2.25 MHz linear array ultrasonic transducer having 128 elements with the element pitch of 0.75 mm was used in both simulation and experiments. In case of Virtual Source-Full Matrix Capture (VSFMC), 8 numbers of elements were used to form the virtual source at a specific depth based on the CIVA simulation studies as detailed in section 3.1. CIVA is a multi-expertise software platform for simulation of multiple-techniques in Non Destructive Testing (NDT) [6]. It is widely used for simulation of complex geometry inspection. An elastodynamic Geometrical Theory of Diffraction (GTD)-Kirchhoff model based on Physical Theory of Diffraction (PTD) has been utilized for simulating response of SDHs and planar defects in CIVA 11 [20, 21]. This model provides a unified modeling of both specular reflection and diffraction phenomena. As mentioned in section 2.1, the vertical planar defects are made to simulate the lack of side wall fusion at the weld-parent metal interface. As the lack of side wall fusion needs to be detected from the parent metal side without the requirement of the ultrasonic beam to enter in the weld zone, the response of these defects made in the quasi-isotropic forge block can be considered close to the side wall fusion in a weld. Further, the grain size in Alloy 617 forging block is of the order of 0.2 mm i.e. about $1/10^{th}$ of the wavelength used in the present study. Hence, isotropic acoustic property of the calibration block is used in the CIVA 11 simulation. Even though, lack of side wall fusion type defects of very small width could not be practically machined in the test specimen for experimental studies, tight planar defects were simulated in CIVA to obtain the response of such defects in ABVSFMC-TFM with different experimental configurations. In addition to the planar defects, the response of SDHs were also studied in the present study as SDHs could be machined in the calibration block similar to those considered in the simulation. The simulation has been performed using expert mode feature wherein any transmission/reception sequence can be user-defined within

the limit of the maximum number of elements assumed in the transducer. Using the expert mode, delay laws were created for FMC, Normal Beam (NB) VSFMC, ABVSFMC and PWI methods.

Simulations were performed in three different FMC configurations, as shown in Figs. 2a-c. Figure 2a shows the schematic of data acquisition in conventional FMC (CFMC) configuration, where transmission began with the first element and then it was shifted electronically upto the 64^{th} element. The A-scan signals were received by all 64 elements in every transmission sequence, i.e. a total of 64*64 A-scans were generated. Figures 2b and 2c show the schematics of normal and angle beam-VSFMC, where a group of 8 elements were utilized with suitable delay laws to focus the beam at the depth of 2 mm from the top surface of the specimen (2:2 focusing along the X-axis and Z-axis) to obtain a beam at normal and at specific angles to the normal to the top surface, respectively. The active groups of elements were electronically translated by one element after every transmission sequence up to the last 64^{th} element. Thus, a total of 57 (=64-8+1) number of transmission sequences were performed in every VSFMC data acquisition. In every transmission sequence, the signals were received by all 64 elements similar to that in the CFMC reception, i.e. a total of 57*64 A-scans were generated. Simulations were also performed for PWI with the plane waves at angles in the range of 1˚ to 89˚ with the step of 1˚ i.e. a total of 90*64 A-scans were generated.

The experiments were performed using GEKKO phased array ultrasonic equipment supplied by M/s. Eddyfi with the maximum number of 64 simultaneous transmitting and receiving channels. The delay laws generated using CIVA was used for acquiring the data in NBVSFMC and ABVSFMC modes. The raw A-scan signals were saved and the TFM images were generated using a software developed in LabVIEW. The experimental results of ABVSFMC-TFM were also compared with the FMC-TFM and PWI-TFM results obtained directly using the software in the

GEKKO equipment. The ratio of the signal amplitude and the corresponding maximum noise amplitude in the vicinity (within 10 mm) of the defect signal in the same echo-dynamic pattern were used to calculate the SNR.

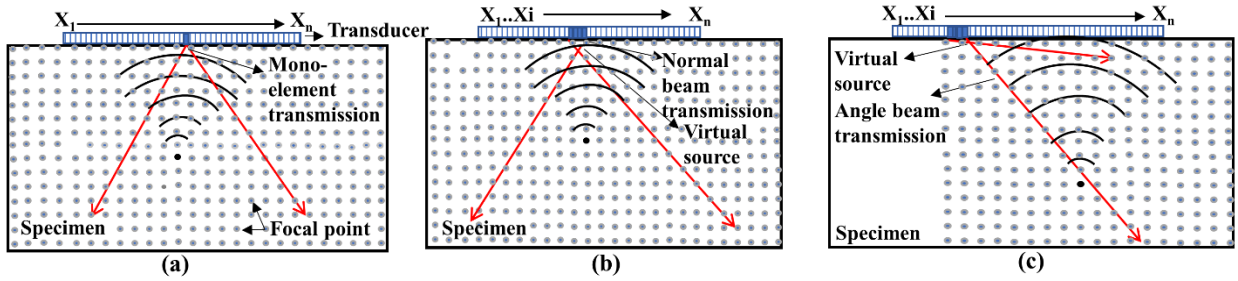

Figure 2. Schematic of transmission in (a) FMC-TFM, (b) NBVSFMC-TFM and (c) ABVSFMC-TFM

3. RESULTS AND DISCUSSION

3.1 CIVA simulations

3.1.1 Beam computation using CIVA simulation

Figure 3 shows the sound beam computation using CIVA 11 software using linear array of 8 active elements with 2.25 MHz, 0.75 mm pitch for different focusing points. Extensive beam computation study has been performed by Nanekar et al. [7] for optimization of number of elements for phased array probes of different frequencies and pitch values for generation of virtual source beam. They utilized the virtual source in a methodology called 'PA-SAFT' combining phased array (PA) with synthetic aperture focusing technique (SAFT). The results showed that the 6 dB beam width decreased with increasing number of elements in the active aperture and it was almost constant beyond 6 or 8 numbers of elements depending upon the pitch and the frequency combinations. Based on this, 8 elements active aperture has been considered in the present study. The acoustic pressure is high near the surface indicated by blue (region:1 in Fig. 3a) in all the cases. The green (region:2 in Fig. 3a) indicates the minimum acoustic pressure. Figure 3a shows

that with focusing at x (horizontal) and y (vertical) positions of 1 mm and 1 mm (1:1), the beam spread is large. However, beam splitting is observed from the main lobe and the acoustic pressure is very low beyond ~40 mm depth. Figure 3c shows that the acoustic pressure is fairly high even at larger depths, but the beam is getting narrower with increasing virtual source distance i.e. losing the beam divergence. Focusing at 2:2 provides a large divergence (~±30˚) with the intended directivity at 45˚. This helps to achieve focusing during the image reconstruction and hence used in the present study.

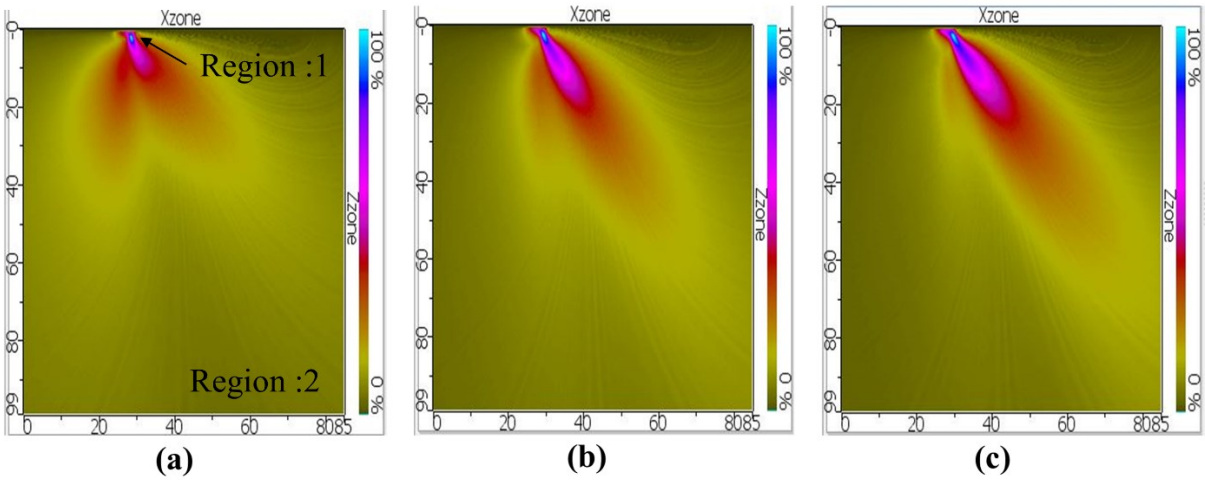

Figure 3. Beam computation results using 2.25 MHz, 0.75 mm pitch for different focusing (a) 1:1, (b) 2:2 and (c) 3:3

3.1.2 Comparison of FMC-TFM, NBVSFMC-TFM and PWI-TFM

Figure 4 shows the TFM images generated in CIVA 11 for different experimental configurations simulated in CIVA. The amplitude range values in the simulation results shown in Figs. 4-7 are different depending upon the maximum amplitude obtained in the specific configuration. However, the amplitude values across different configurations can be compared with each other in the CIVA simulation results, e.g. PWI-TFM (Fig. 4d) exhibits ~20 times higher amplitude as compared to that for the FMC-TFM (Fig. 4a).

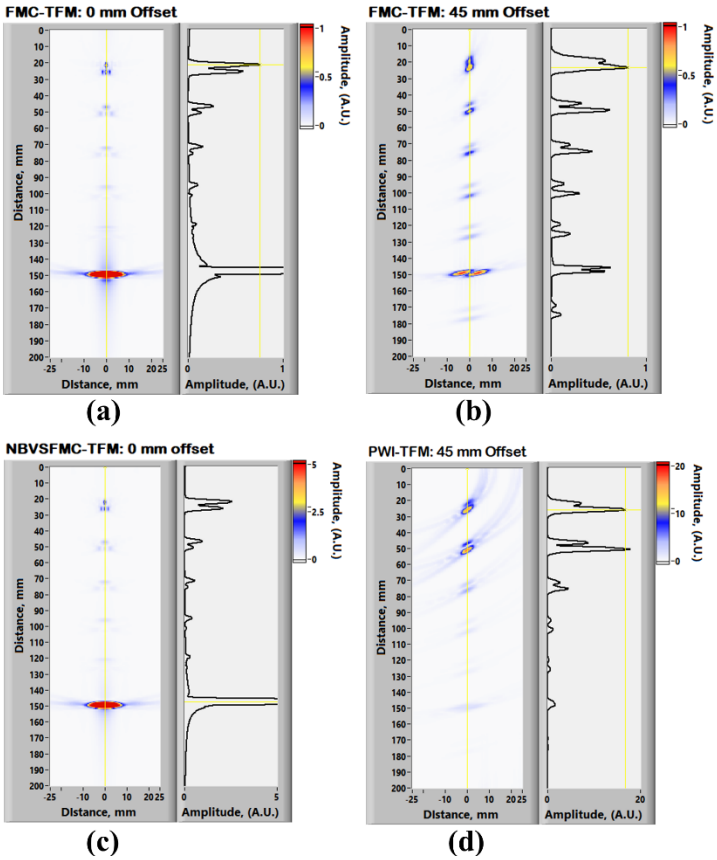

Figure 4. B-scan image using CIVA simulation for a) FMC-TFM, b) FMC-TFM with 45 mm offset, c) NBVSFMC-TFM and d) PWI with 45 mm offset

Figure 4a shows the simulated FMC-TFM image obtained for the reference block shown in Fig. 1 by considering the transducer on top of the defect. The amplitude of the deeper defects decrease drastically as compared to the near surface defect located at 25 mm from the top surface. In order to study the response of the planar defects using angle beam FMC-TFM, the transducer was kept at 45 mm offset from the centre line of the defects. Figure 4b shows the TFM B-scan image with improved amplitude for the deeper defects as compared to that in the normal beam FMC-TFM (Fig. 4a). Further, the bottom tip indicated higher amplitude, in general, as compared to the top tip of the defects in angle beam inspection simulation.

Single element provides less acoustic energy which may not be sufficient for the detection of deeper defects with higher amplitude and a required SNR. With increase in the number of

elements to 8 in the VSFMC-TFM, the acoustic energy increases. The amplitude is increased by about 4 times in the NBVSFMC-TFM (Fig. 4c) as compared to that in the FMC-TFM (Fig. 4a) for the transducer considered on top of the defect in both the cases. Figure 4d shows PWI-TFM B-scan image obtained by angles of transmission in the range of 1˚ to 89˚. It can be seen that the amplitude is higher for defects near the top surface due to higher acoustic energy and decreases drastically with increasing depth for defects at 75 mm and beyond. It should be noted in Fig. 4 that the amplitude range is 0-1 A.U. in Figs. 4a (FMC) and 4b (FMC with 45 mm probe offset), whereas it is 0-5 A.U. in Fig. 4c (NBVSFMC) and 0-20 A.U. in Fig. 4d (PWI). The horizontal defect at 150 mm depth shows very high amplitude in normal beam inspections (Figs. 4a and 4c). These simulation studies clearly indicated about 4 times and 20 times increase in amplitude in VSFMC-TFM and PWI-TFM, respectively as compared to FMC-TFM. Further, it is also observed that the bottom tips can be clearly resolved only by performing angle beam inspections.

3.1.3 ABVSFMC-TFM with different incidence angles

The ABVSFMC-TFM provides the possibility of directing the beam at the desired angles and thus enhancing the sensitivity at the desired depths in angle beam inspection for a given probe offset position. In order to detect the diffracted signals with improved sensitivity throughout the thickness, simulation was performed for different beam angles for 45 mm offset. Figures 5 a-d show TFM B-scan images and corresponding echo-dynamic patterns for ABVSFMC-TFM for 70˚, 60˚, 30˚ and 15˚ beam angles, respectively. It is observed that as the incidence angle decreases, the amplitude of the diffracted signals from the deeper defects increase due to the incident angle beam hitting the deeper defects directly. To detect the diffracted signals with improved sensitivity at

specific depth and probe offset distance, suitable beam angle can be selected in the ABVSFMC-TFM.

3.2 Comparison of CIVA simulation with experimental results

Figures 6 a and b show the CIVA simulation and experimental results, respectively for the response of SDHs (Fig. 1b) in ABVSFMC-TFM with 45˚ incidence beam and ~50 mm probe offset. The maximum amplitude in the experimental ABVSFMC-TFM is normalized to the maximum amplitude in the CIVA simulation result (0-40 A.U.). Both exhibit similar trend except for a rapid drop in the amplitude with increasing defect depth in the experimental results. This is attributed to the attenuation in alloy 617 block which is not considered in the CIVA simulation.

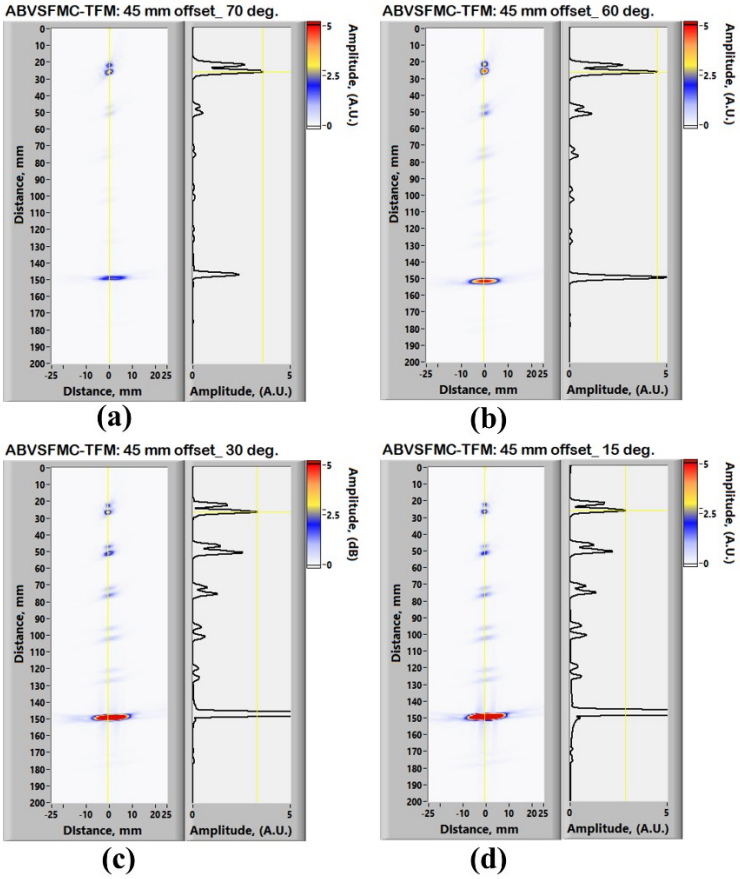

Figure 5. TFM B-scan image obtained by CIVA simulation using ABVSFMC-TFM for (a) 70˚ angle, (b) 60˚ angle, (c) 30˚ angle and (d) 15˚ angle

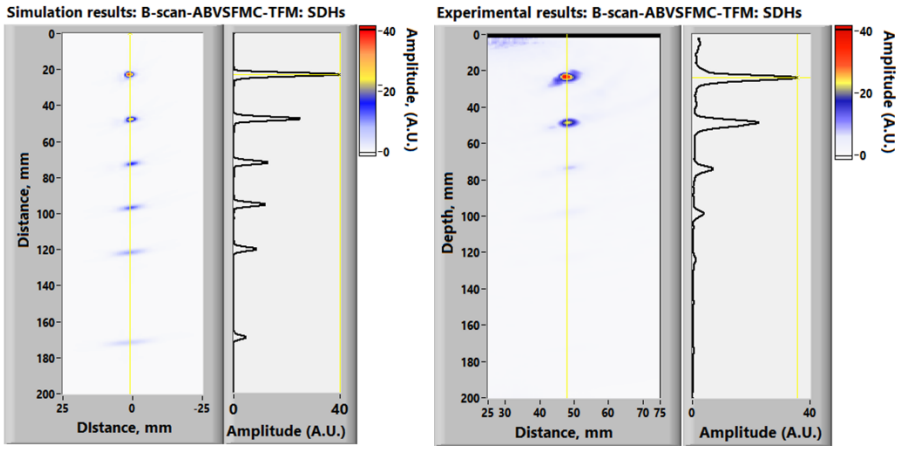

(a) (b)

Figure 6. (a) simulation and (b) experimental (gain=50 dB) B-scan images and echo-dynamic patterns for SDHs at various depths obtained using ABVSFMC-TFM with the probe offset of ~50 mm

Figure 7a shows the CIVA simulation result of ABVSFMC-TFM with ~50 mm probe offset for the planar defects. The amplitude of the tip diffracted signals for the planar defects are observed to be about 10 times lower as compared to the SDHs at the same defect depth in the CIVA simulation. However, the amplitude is only about 5 times lower for the tip diffracted signals in the experimental results as compared to the SDHs. Further, the experimental results indicated the highest amplitude for the defect at 50 mm depth due to the beam directed at 45˚, unlike the CIVA simulation results that indicated maximum amplitude for the defect at 25 mm depth. This difference may be attributed to the effect of the width of planar defects on the angle specific tip diffracted signals in the two cases. Further, higher amplitude is observed for the horizontal defect at 150 mm depth in the CIVA simulation as compared to that in the experimental result.

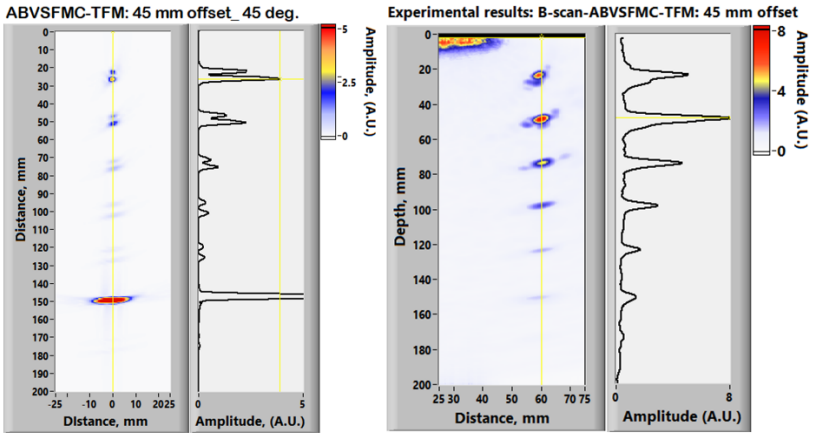

Figure 7. (a) Simulation and (b) experimental (gain=50 dB) B-scan images and echo-dynamic patterns for planar defects at various depths obtained using ABVSFMC-TFM with the probe offset of ~50 mm

3.3 Comparison of experimental results for FMC-TFM, PWI-TFM and ABVSFMC-TFM

Figure 8 shows the B-scan images and corresponding A-scan signals for vertical slots obtained using FMC-TFM (without probe offset), PWI-TFM (with ~80 mm offset) and ABVSFMC-TFM (with ~80 mm offset) at 70 dB, 52 dB and 50 dB instrument gain, respectively. It can be seen in Fig. 8a that only the near surface defects up to the depth of 50 mm could be detected clearly in FMC-TFM. Whereas, in PWI-TFM and ABVSFMC-TFM, all the defects could be detected clearly with higher sensitivity (Figs. 8 b and c). In PWI-TFM, all the top and bottom tip signals are clearly seen (Fig. 8b) except for the defect at 175 mm depth, for which only the top tip signal could be detected. All slots could be reliably detected using ABVSFMC-TFM with 80 mm probe offset. It can be seen in Fig. 8 that the PWI and ABVSFMC-TFM exhibited similar amplitude at about 20 dB lower gain as compared to FMC-TFM. The increased sensitivity in PWI and ABVSFMC-TFM are attributed to the increased number of transmitting elements in the aperture. Even though the number of transmitting elements is only 8 ($1/8^{th}$ of that in the PWI) in

the case of ABVSFMC-TFM, similar amplitudes observed in PWI and ABVSFMC-TFM is attributed to the directivity of the beam with good divergence in the intended direction.

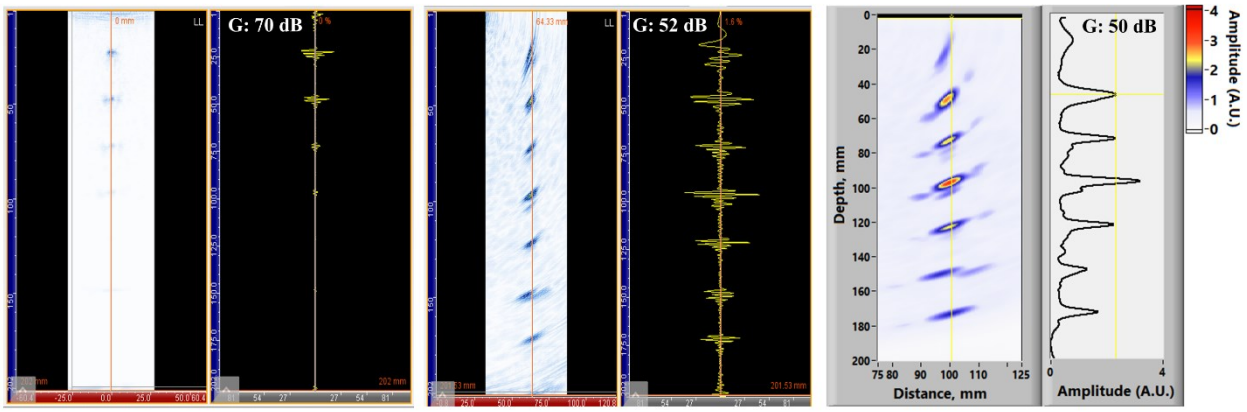

Figure 8. B-scan and echo dynamic pattern for inconel specimen for slots using (a) FMC-TFM (no offset), (b) PWI-TFM (80 mm offset) and (c) ABVSFMC-TFM (80 mm offset)

The signal to noise ratio (SNR) obtained using FMC-TFM, ABVSFMC-TFM and PWI are compared for slots at different depths in Fig. 9. The SNR decreased with increasing depth of defect for the probe offset of 45 mm for all the techniques. Further, both PWI and FMC-TFM exhibited similar SNR for 45 mm probe offset, whereas, the ABVSFMC-TFM exhibited ~6 dB higher SNR. For the probe offset of 80 mm, the SNR is observed to be better than those observed for the probe offset of 45 mm for the defects at larger depths in ABVSFMC-TFM. This is attributed to larger divergence with directivity of the beam leading to defect information in large number of A-scan signals. This results in improved SNR upon application of TFM algorithm.

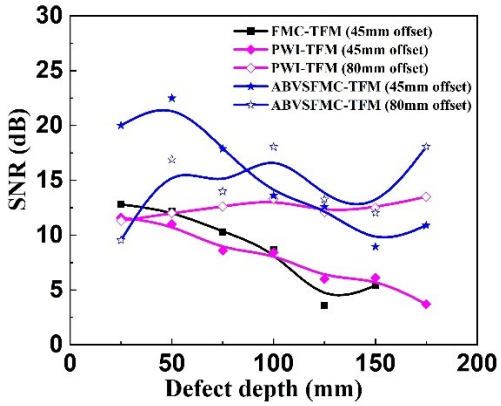

Figure 9. Variations in SNR as a function of defect depth for different experimental configurations

4. CONCLUSIONS

TFM based ultrasonic phased array imaging techniques with different data acquisition methodologies such as conventional FMC, NBVSFMC, ABVSFMC and PWI have been explored through CIVA simulation in the present study for inspection of thick components. The use of single element transmission exhibited lower amplitude in case of conventional FMC-TFM, particularly at larger depths. The benefit of transmission using multiple elements was evident in PWI imaging of defects at larger depths. Advantages of a newly proposed method ABVSFMC-TFM was demonstrated against both FMC-TFM and PWI-TFM for specific cases. The study also demonstrates that with suitable positioning of the transducer and the incidence angle, sensitivity can be tailored in the ABVSFMC-TFM technique for specific depth. The CIVA results of FMC-TFM is found to be in good agreement with the experimental results on a 200 mm thick forged Alloy 617 specimen with side drill holes at different depths. For the planar defects, the experimental results indicated some deviation from the CIVA simulation results which is attributed to the different width of the defects considered in the simulation and experiments. The study indicates that ABVSFMC-TFM can be considered as a promising technique for angle beam

inspection of thick and attenuating materials with the advantage of beam divergence with directivity in the intended direction.

REFERENCES

[1]. Holmes C., Drinkwater B.W., and Wilcox P.D., *Advanced post-processing for scanned ultrasonic arrays: Application to defect detection and classification in non-destructive evaluation*. Ultrasonics, 2008. **48**(6-7): p. 636-642.

[2]. Holmes C., Drinkwater B.W., and Wilcox P.D., *Post-processing of the full matrix of ultrasonic transmit–receive array data for non-destructive evaluation*. NDT & E International, 2005. **38**(8): p. 701-711.

[3]. Nanekar P., Kumar A., and Jayakumar T., *Characterization of planar flaws by synthetic focusing of sound beam using linear arrays.* Case Studies in Nondestructive Testing and Evaluation, 2015. **3**: p. 9-14.

[4]. Karaman M., Li P.-C., and O'Donnell M., *Synthetic aperture imaging for small scale systems. IEEE transactions on ultrasonics, ferroelectrics, and frequency control*, 1995. **42**(3): p. 429-442.

[5]. Sutcliffe M., Weston M., Charlton P., Dutton B., and Donne K., *Virtual source aperture imaging for non-destructive testing.* Insight-Non-Destructive Testing and Condition Monitoring, 2012. **54**(7): p. 371-379.

[6]. Sutcliffe M., Charlton P., and Weston M., *Multiple virtual source aperture imaging for non-destructive testing.* Insight-Non-Destructive Testing and Condition Monitoring, 2014. **56**(2): p. 75-81.

[7]. Alavudeen S., Krishnamurthy C., and Balasubramaniam K. *Technique for Imaging using Virtual Array of Sources (TIVAS)*, in AIP Conf. Proc. July 18-23, 2010, San Diego, California, 2011. AIP. **1335**: p. 1687-1694.

[8]. Bannouf S., Robert S., Casula O., and Prada C. *Data set reduction for ultrasonic TFM imaging using the effective aperture approach and virtual sources*. in Journal of Physics: Conference Series. IOP Publishing, 20-23 June 2014, Chengdu, 2013. **457**: p. 012007.

[9]. Zhang X., Guo J., Luo X., Gao X., Wang Z., Zhao Q., and Zheng B. *Defect detection study on total focus method of sound field imaging based on parallel processing*. in *Nondestructive Evaluation/Testing (FENDT), 2014 IEEE Far East Forum on*. 20-23 June 2014, Chengdu, China. p.112-116.

[10]. Lookwood G. and Foster F.S., Optimizing the radiation pattern of sparse periodic two-dimensional arrays. IEEE transactions on ultrasonics, ferroelectrics, and frequency control, 1996. **43**(1): p. 15-19.

[11]. Spencer R., Sunderman R., and Todorov E. *FMC/TFM experimental comparisons*. in AIP Conf. Proc. AIP Publishing, 16-21 July 2017, Provo, Utah, USA, **37**: p. 020015-1–020015-5.

[12]. Long R., Russell J., Cawley P., and Habgood N. *Ultrasonic phased array inspection of flaws on weld fusion faces using full matrix capture*. in AIP Conf. Proc. 22-25 July 2008, Chicago, Illinois, 2009. **28**: p. 848-855.

[13]. Le Jeune L., Robert S., and Prada C. *Plane wave imaging for ultrasonic inspection of irregular structures with high frame rates*. in AIP Conf. Proc. 26-31 July 2015, Minneapolis, Minnesota, 2016. **1706**: p. 020010.

[14]. Le Jeune L., Robert S., Villaverde E.L., and Prada C. *Multimodal plane wave imaging for non-destructive testing*. in 2015 ICU International Congress on Ultrasonics, 1 Jan., France, 2015. **70**: p. 570 – 573.

[15]. Matrone G., Savoia A.S., Caliano G., and Magenes G. *Ultrasound plane-wave imaging with delay multiply and sum beamforming and coherent compounding*. in Engineering in Medicine and Biology Society (EMBC), 2016 IEEE 38th Annual International Conference of the. 2016. IEEE. 16 Aug., Orlando, USA, p. 3223-3226.

[16]. Le Jeune L., Robert S., Lopez Villaverde E., and Prada C., *Plane Wave Imaging for ultrasonic non-destructive testing: Generalization to multimodal imaging*. Ultrasonics, 2016. **64**: p. 128-138.

[17]. Long R., Russell J., and Cawley P. *Through‐weld ultrasonic phased array inspection using full matrix capture*. in AIP Conf. Proc. 26-31 July 2009, Kingston, 2010. **1211**(1): p. 918-925.

[18]. Payão Filho J., Passos E., Gonzaga R., Ferreira R., Santos D., and Juliano D., *Ultrasonic Inspection of a 9% Ni Steel Joint Welded with Ni-based Superalloy 625: Simulation and Experimentation*. Metals, 2018. **8**(10): p. 787.

[19]. Mahaut S., Darmon M., Chatillon S., Jenson F., and Calmon P., *Recent advances and current trends of ultrasonic modelling in CIVA*. Insight-Non-Destructive Testing and Condition Monitoring, 2009. **51**(2): p. 78-81.

[20]. Dorval V., Darmon M., Chatillon S., and Fradkin L. *Simulation of the UT inspection of planar defects using a generic GTD-Kirchhoff approach*. in AIP Conf. Proc. 2015. American Institute of Physics. 20-25 July 2014, Boise, Idaho, 2015. **1650**(1): p. 1750-1756.

[21]. Mahaut S., Lonne S., and De Roumilly L., *Validation of CIVA simulation tools for ultrasonic inspection in realistic configuration*. ENDT, 2006: p. 1-8.

[22]. Nanekar P., Kumar A., and Jayakumar T., *SAFT-assisted sound beam focusing using phased arrays (PA-SAFT) for non-destructive evaluation*. Nondestructive Testing and Evaluation, 2015. **30**(2): p. 105-123.